Materials Today Bio 13 (2022) 100187

Contents lists available at ScienceDirect

Materials Today Bio

journal homepage: www.journals.elsevier.com/materials-today-bio

Bioactive fluorescent hybrid microparticles as a stand-alone osteogenic differentiation inducer

Neda Aslankoohi [a], Shigang Lin [b], Kibret Mequanint [a,b,*]

[a] School of Biomedical Engineering, The University of Western Ontario, London, Ontario, N6A 5B9, Canada
[b] Department of Chemical and Biochemical Engineering, The University of Western Ontario, London, Ontario, N6A 5B9, Canada

ARTICLE INFO

Keywords:
Organic-inorganic fluorescent hybrid microparticles
Sol-gel process
poly(ester amide)s
Bioactive glass
Dexamethasone delivery
Osteogenic differentiation

ABSTRACT

Osteogenic differentiation of stem cells is one of the essential steps in bone regeneration. While supplementing exogenous factors using differentiation media is the established method to differentiate stem cells into osteoblasts on biomaterials, designing biomaterials that can act as a stand-alone differentiation inducer and promote bone regeneration is preferred for clinical translation. In this work, we report dexamethasone-loaded organic-inorganic hybrid microparticles synthesized from an intrinsically fluorescent poly (ester amide) and tertiary bioactive glass (PEA-BG) as a stand-alone osteogenic differentiation inducer. The mechanical properties data indicated that the compressive modulus of fluorescent hybrid microparticles could be modulated by its composition. The hybrid fluorescent microparticles supported the adhesion and proliferation of 10T1/2 cells in culture for up to seven days. Both pristine and dexamethasone-loaded PEA-BG microparticles were able to induce osteogenic differentiation of 10T1/2 cells in the absence of any media supplement, to a level even higher than standard osteogenic media, as evidenced by the expression of osteogenic markers on gene and protein levels and matrix mineralization. Taken together, the fluorescent PEA-BG hybrid microparticles have the potential to be used as a stand-alone biomaterial for osteogenic differentiation and bone regeneration.

1. Introduction

Attempts made so far in bone tissue engineering relied on either the delivery of stem cells through implantation of cellularized scaffolds or hydrogels or recruitment of endogenous stem cells after implantation of an acellular scaffold. In both approaches, differentiation of implanted exogenous or recruited endogenous stem cells to osteogenic lineage is essential for bone repair and regeneration. *In vitro* studies to evaluate the differentiation of stem cells in the presence of biomaterials are mostly conducted using osteogenic media, which is a cocktail of growth medium and three mediators, namely ascorbic acid, dexamethasone, and β-glycerophosphate. However, these mediators are notably absent *in vivo* [1] and hence, these *in vitro* experimental conditions do not predict the actual *in vivo* fate of the biomaterials and cells. Moreover, even if the implantation of pre-differentiated cellular scaffolds is considered, the use of these osteogenic mediators may confound the real effect of biomaterials [2]. To close this gap, different strategies for induction of differentiation by biomaterials in the absence of media supplements, such as the use of growth factors (e.g., bone morphogenic proteins) or synthetic peptide analogs [3], geometrical and topographical cues affecting the cell fate [4] and their combination with growth factors [5], and the use of co-culture to mimic the cellular niche of tissue [1] have been investigated.

Bioactive glasses (BG) have long been studied for their osteoconductive potential stemming from the release of stimulatory ions [2]. The sol-gel chemistry provides the possibility of doping the bioactive glasses with different ions to provide cues for desired cell responses. The combined delivery of stimulatory ions of bioactive glasses and osteogenic factor(s) have also been studied to promote bone regeneration [6–8]. In terms of morphology, particulate morphology specifically provides flexibility for filling bone defects of different shapes and sizes, offers a higher surface area for cell-material interaction, and can be incorporated into injectable formulations. Recent studies have shown the ability of BG nanoparticles to direct cells towards osteogenic lineage in the absence of media supplements through the release of different ions such as calcium, phosphate, and strontium ions [9,10]. It has been shown that a single dose of mesoporous silica nanoparticles loaded with dexamethasone and functionalized with calcium and phosphate ions could induce osteogenic differentiation in human bone marrow mesenchymal stem cells [8]. However, several studies have also reported that silica/bioactive glass particles or their extracts can only enhance osteogenic differentiation of

* Corresponding author. Department of Chemical and Biochemical Engineering, The University of Western Ontario, London, Ontario, N6A 5B9, Canada.
E-mail address: kmequani@uwo.ca (K. Mequanint).

https://doi.org/10.1016/j.mtbio.2021.100187
Received 1 October 2021; Received in revised form 7 December 2021; Accepted 8 December 2021
Available online 9 December 2021

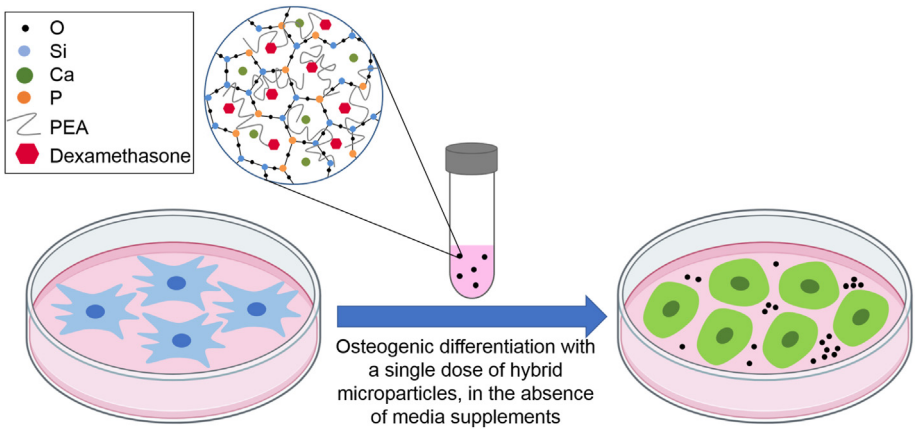

Scheme 1. Schematic illustration of experimental design. Pristine or dexamethasone-loaded PEA-BG hybrid microparticles are added to the media in a single dose to induce osteogenic differentiation.

cells in the presence of differentiation media rather than inducing osteogenic differentiation without additional osteogenic supplements [11,12]. While a direct comparison between different studies is not possible due to differences in cell types, BG composition, its concentration in media, treatment duration, and exposure of cells to the biomaterial or its extracts, it can be concluded that inorganic glasses can be exploited for osteoconductivity. The inclusion of an organic phase in the form of a hybrid biomaterial can introduce additional functionalities. However, the sol-gel reaction conditions frequently used to prepare nano and micro bioactive glass particles either utilize highly alkaline conditions and/or need a post-synthesis calcination step to remove surfactants used in the synthesis, which neither is compatible with biodegradable polymers. Previously, we introduced a versatile synthesis approach for the preparation of fluorescent bioactive and biodegradable polymer-BG hybrid microparticles with the possibility of dual-drug loading during synthesis [13]. Herein, we investigated the potential of these polymer-BG hybrid microparticles, having intrinsically fluorescent poly (ester amide) (PEA) as their polymer component, in their pristine form or loaded with a known osteogenesis inducing factor, dexamethasone, to differentiate murine embryonic mesenchymal progenitor cells (10T1/2 cells) into osteogenic lineage as a stand-alone system (Scheme 1).

2. Materials and methods

2.1. Materials

Tetraethyl orthosilicate (TEOS, 98%), triethyl phosphate (TEP, 99.8%), dexamethasone, Alizarin Red S, and L-ascorbic acid were purchased from Sigma-Aldrich (Milwaukee, WI, USA). Dimethylformamide (DMF) was purchased from Caledon Laboratory Chemicals (Georgetown, ON, Canada). Methyl ethyl ketone (MEK) and calcium chloride dihydrate were purchased from Fisher Scientific. The poly (ester amide) (PEA), named 8-Phe-4, was synthesized by interfacial polymerization according to our previous publication [14], using sebacoyl chloride, L-phenylalanine, and butanediol.

2.2. Synthesis of organic-inorganic hybrid microparticles

Sol-gel process in the presence of organic phase was conducted to obtain hybrid microparticles (MPs) according to our previous publication [13]. Briefly, a known amount of PEA was dissolved in DMF and MEK. The ratio of organic to inorganic components was kept at 50 wt%, and the inorganic component was tertiary bioactive glass with a molar composition of either 70% SiO_2-10% $CaCl_2$-20% P_2O_5 [Hybrid (70Si)] or 85% SiO_2-10% $CaCl_2$-5% P_2O_5 [Hybrid (85Si)]. An inorganic sol was prepared separately at room temperature (RT) and then was added to the PEA solution. After complete mixing, the solution was kept at 60 °C until gelation, followed by drying under vacuum at 60 °C. For dexamethasone-loaded microparticles, first, 100 mg PEA was dissolved in 1.5 mL DMF/MEK. To this solution, 1.3 mg dexamethasone was added prior to mixing with the inorganic sol, resulting in microparticles with 0.6 wt% loaded dexamethasone.

2.3. Characterization of hybrid microparticles

The morphology of the hybrid was visualized using scanning electron microscopy (LEO 1540XB SEM, Hitachi, Japan). Samples were mounted on a sample holder using carbon tape and then sputter-coated with gold/palladium (K550X sputter coater, Emitech Ltd., UK) prior to visualization. To measure the *in vitro* release profile of dexamethasone, hybrid microparticles were incubated in phosphate-buffered saline (PBS) at 37 °C with shaking at 120 rpm. At a pre-determined time point, aliquots were removed and replaced with fresh pre-warmed PBS. Released dexamethasone at each time point was analyzed with UV-VIS spectrophotometer at 242 nm. The experiments were conducted in triplicate.

2.4. Evaluation of mechanical properties

To evaluate the mechanical properties, cylindrical specimens (6 mm diameter and 9 mm height) were prepared from hybrid microparticles and PEA using compression molding in a custom-made stainless-steel mold (1 MPa, 100 °C, 1 h). Instron Universal Mechanical testing machine was used to conduct a uniaxial compression testing with a 5 kN load cell, 10 N pre-loading, and a crosshead speed of 1 mm/min ($n = 5$ for hybrids, and $n = 3$ for PEA controls). The slope of the linear portion of the stress-strain curve was reported as compressive modulus. The modulus of toughness was determined as the area under the stress-strain curve up to the point of 30% strain.

2.5. In vitro cell culture with hybrid microparticles

Embryonic multipotent mesenchymal-like progenitor cell line (10T1/2 cells) (ATCC) were cultured in Dulbecco's Modified Eagle's Medium (DMEM) (Thermo Fisher) containing 5% Fetal Bovine Serum (FBS) (Thermo Fisher) and 1% penicillin/streptomycin. Cells were seeded in a 24-well plate with a seeding density of 5×10^4 per well. After reaching confluency, the cell culture media was aspirated and replaced with either media containing PEA-BG microparticles, disinfected by exposure to UV light for 10 min, or osteogenic media, depending on the experimental design. For all experiments evaluating the differentiation of cells, pristine or dexamethasone-loaded hybrid (70Si) microparticles with a concentration of 5 mg/mL microparticles were used. For cell metabolic activity

and proliferation measurements, hybrid (85Si) microparticles were used. Osteogenic media contained 10^{-7} M dexamethasone, 50 μg/mL ascorbic acid, and 3 mM $Na_xH_{3-x}PO_4$. Cells cultured with DMEM media and DMEM media containing 10^{-7} M dexamethasone were used as controls. The medium was changed every 3 days. At least three replicates were used for each experiment. For staining purposes, a glass slide was inserted at the bottom of wells prior to cell seeding. After a pre-determined time, cells were fixed using 4% paraformaldehyde (PFA) (EMD Chemicals Inc. Gibbstown, NJ) and stained with Alexa-Fluor 568 conjugated phalloidin (1:100; Thermo Fisher) to visualize F-actin and counterstained with 4′,6-diamidino-2-phenylindole (DAPI, 300 nM in PBS, Thermo Fisher, Canada) for labeling nuclei. Images were taken with a Zeiss LSM 800 confocal microscope (Zeiss, Canada).

2.6. 10T1/2 cells adhesion to hybrid biomaterial

To investigate the adhesion of cells to the hybrid microparticles, a layer of hybrid was applied on glass slides by dipping them three times in hybrid solution followed by drying at 60 °C under vacuum. The samples were disinfected by immersion in 70% ethanol for 30 min followed by two washes with HBSS and subsequently 15,000 cells/cm^2 were seeded. 10T1/2 cells cultured on glass slides were used as a control. To visualize focal adhesion of the cells after a pre-determined time, cells were fixed using 4% PFA and then were permeabilized for 10 min with 0.1% Triton X-100 in PBS and rinsed three times with PBS. Cells were then blocked with 1% BSA in PBS for 30 min at ambient temperature, followed by overnight incubation (at 4 °C) with anti-vinculin antibody (1:50; MAB3574, clone VIIF9, EMD Millipore). The primary antibody binding was detected using Alexa Fluor 594 goat anti-mouse IgG as a secondary antibody (1:300; Thermo Fisher, Canada). The cells were counterstained with DAPI for labeling nuclei. To visualize the cytoskeleton, cells were stained with Alexa-Fluor 568 conjugated phalloidin (1:100) and counterstained with DAPI. Images of single cells with labeled F-actin were used to determine cell area using ImageJ software. Images of cells with labeled vinculin were used to determine the number of focal adhesions per cell using the particles analysis feature of ImageJ software with an area threshold of 0.1–0.5 μm^2 [15]. The area threshold was selected to include only vinculin-labeled areas associated with focal adhesions at the periphery of the cells and exclude perinuclear vinculin not involved in focal adhesion points.

2.7. Metabolic activity and proliferation of cells

The metabolic activity of the cells was measured using MTT assay (Sigma-Aldrich), following the manufacturer's protocol, and the absorbance was measured using an Asys UVM 340 plate reader at a wavelength of 570 nm with reference to 680 nm. To measure cell proliferation, CyQuant cell proliferation assay kit (Invitrogen, Canada) was used according to the manufacturer's protocol, and the fluorescence intensity was measured with a Tecan Infinite M1000 Pro fluorescence plate reader.

2.8. Osteogenic gene expression of 10T1/2 cells

For osteogenic gene expression experiments, after a pre-determined culture time, total RNA was extracted using Trizol (Thermo Fisher) following the manufacturer's protocol. Complementary DNA (cDNA) template was prepared by using 1 μg of total RNA primed with random primers according to Promega™ Random Hexamers protocol (Thermo Fisher). qPCR was carried out in 10 μL of reaction volumes, using a CFX96™ Real-Time System (C1000 Touch Thermal Cycler; Bio-Rad, Canada) and then measured with iQ™ SYBR® Green Supermix (Bio-Rad) according to the recommended protocol by the manufacturer. The sequences of primers were designed using Primer3Web and are presented in Table 1. The results were analyzed with the comparative threshold cycle method and normalized with GAPDH as an endogenous reference and reported as relative values (ΔΔ CT) to the negative control.

Table 1
Primers for mouse-specific mRNA amplification.

Gene	Forward primer (5′→ 3′)	Reverse primer (5′→ 3′)
Alpl	CCTTCACGGCCATCCTATATG	CTGGTAGTTGTTGTGAGCGTA
Spp1	ATCTCACCATTCGGATGAGTCT	TGTAGGGACGATTGGAGTGAAA
Runx2	CACTGGGTCACACGTATGATT	AGGGAAGGGTTGGTTAGTACA
Bglap	GGCCCAGACCTAGCAGACAC	TTGCCCTCCTGCTTGGACAT
IBSP	GAGCCAGGACTGCCGAAAGGAA	CCGTTGTCTCCTCCGCTGCTGC
Sp7	GCCAGTAATCTTCAAGCCAGA	CCATAGTGAGCTTCTTCCTGG
GAPDH	GGTGGTCTCCTCTGACTTCAACA	GTTGCTGTAGCCAAATTCGTTGT

Alp1 - Alkaline phosphatase; *Spp1* - Osteopontin; *Runx2* - Runt-related transcription factor 2; *Bglap* - Bone gamma carboxyglutamate protein; *IBSP* - Bone sialoprotein; *Sp7* - Osterix.

2.9. Western blot analysis

Western blotting was performed to evaluate levels of osteogenic proteins. Briefly, after culturing for 7 days or 14 days, 10T1/2 cells were lysed in buffer containing 150 mM NaCl, 10 mM Tris-HCl (pH 7.4), 1 mM EDTA, 0.5% Nonidet P-40, and 1% Triton X-100 and supplemented with protease inhibitor (Roche Applied Science, Indianapolis, IN, USA). Protein concentrations were determined by Quick Start™ Bradford Protein Assay (Bio-Rad, Mississauga, ON, Canada), and 20–200 μg of total protein lysate was resolved on 12% SDS-PAGE and subsequently transferred to nitrocellulose membrane. The proteins of interest were immunoblotted using the following primary antibodies: anti-Osteopontin (rabbit, 1:2000; Abcam, ab8448) and anti-Osteocalcin (rabbit, 1:250; Abcam, ab133612). Primary antibody labeling was detected using HRP-conjugated goat anti-rabbit secondary antibody and the ECL detection system.

2.10. Evaluation of mineralization

To assess mineralization, cultured cells were fixed with 70% ethanol followed by washing with PBS and water and incubation with a solution of 40 mM alizarin red S (pH = 4.2). After 30 min incubation at RT in the dark, samples were washed three times with water, 15 min each time, under gentle shaking. The stained samples were then visualized by an optical microscope. To quantify the amount of alizarin red, samples were incubated for 30 min with 10% acetic acid. Then, the cell monolayer was scraped and transferred to a centrifuge tube, vortexed for 30 s, overlaid with mineral oil, and heated to 85 °C for 10 min, followed by transferring to ice bath for 5 min. The samples were then centrifuged, and the supernatants were transferred to a clean tube. The pH of each sample was adjusted to 4.1–4.5 using 10% ammonium hydroxide. Finally, the absorbance was measured at 405 nm [16]. Hybrid microparticles incubated in PBS in the absence of cells for the indicated durations, while refreshing PBS every 3 days (similar to cell culture media refreshment) were used as a control to evaluate the amount of alizarin red, if any, due to the microparticles solely.

2.11. Statistical analysis

Data were presented as means ± standard deviations (SD). Statistical significance was calculated using one-way ANOVA with Tukey's post hoc multiple comparison tests. For statistical significance, a p-value of <0.05 was used.

3. Results and discussion

3.1. Synthesis and characterization of dexamethasone-loaded organic-inorganic hybrid microparticles

Fig. 1 shows pristine and dexamethasone-loaded PEA-BG hybrid microparticles having a spherical morphology with a smooth surface topography (Fig. 1A and B). Dexamethasone loading during the synthesis

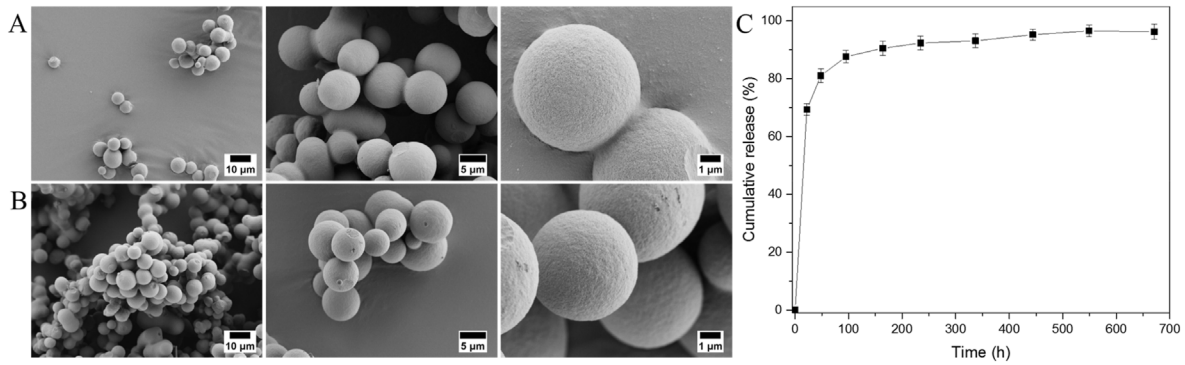

Fig. 1. Morphology of **(A)** Pristine and **(B)** Dexamethasone-loaded PEA-BG hybrid microparticles **(C)** *In vitro* release profile of dexamethasone-loaded microparticles.

reduces the overall complexity of the loading process, and the procedure could easily be adapted for the loading of two compounds (one loaded to the PEA and another loaded to the BG). Here dexamethasone was loaded in the microparticles during their synthesis and showed a burst release of 69%, followed by a continuous release for more than 20 days (Fig. 1C). Similar release kinetics were reported previously for dexamethasone-loaded carriers such as mesoporous silica nanoparticles [8,17] and titanium nanotubes [18]. Functionalization of PEA to conjugate bioactive molecules has been previously reported [19] and could be utilized to gain more control on the release rate of the microparticles.

3.2. Evaluation of mechanical properties

Fig. 2A shows the stress-strain curves for hybrid materials and PEA. The hybrid materials showed an initial elastic deformation up to the yield stress, followed by plastic deformation. The presence of the inorganic phase in the hybrid resulted in enhanced compressive modulus (214.4 ± 32.4 MPa and 319.6 ± 49 MPa) compared to the PEA alone (178.7 ± 29.4 MPa) (Fig. 2B). Comparing the two hybrid materials with different inorganic phase compositions revealed that the hybrid with higher silica content had higher compressive modulus (Fig. 2B). In contrast to modulus, there was no significant difference in toughness between PEA and hybrids (Fig. 2C). The organic content of the hybrid, the molecular weight and structure of the organic phase [20], the composition of the inorganic phase, and the interaction between organic and inorganic phases [21] are among factors affecting the mechanical properties of hybrid materials.

Previously reported PCL-BG hybrid with similar composition had shown higher compressive modulus compared to PEA-BG. This can be due to the higher measured mechanical strength of PCL in comparison to PEA, in light of its higher molecular weight compared to the PEA tested here [22]. Hybrids of silica and poly (CL-co-GPTMS) with 60% organic content showed similar compressive modulus and ultimate stress as the PEA-BG hybrid [23]. It has been shown that the compressive modulus decreases while the strain at failure increases by increasing the organic content of poly (CL-co-GPTMS)-silica and PCL-BG hybrids [22,23]. Both hybrids studied here have 50% PEA; therefore, the significant difference in compressive modulus of them stems from the composition of the inorganic phase. With the incorporation of 10% $CaCl_2$, the compositions difference lies in the silica and phosphorous contents. PEA-BG (85Si) having 85% silica showed a higher compressive modulus. Both Si and P are considered to be network formers in the inorganic structures; however, ^{29}Si and ^{31}P NMR studies of the sol-gel bioactive glasses have shown that phosphorous predominately appears as orthophosphate ions, charge-balanced with cations such as Ca^{2+} and Na^{+} [24,25]. In the absence of sufficient network modifier cations or the presence of other

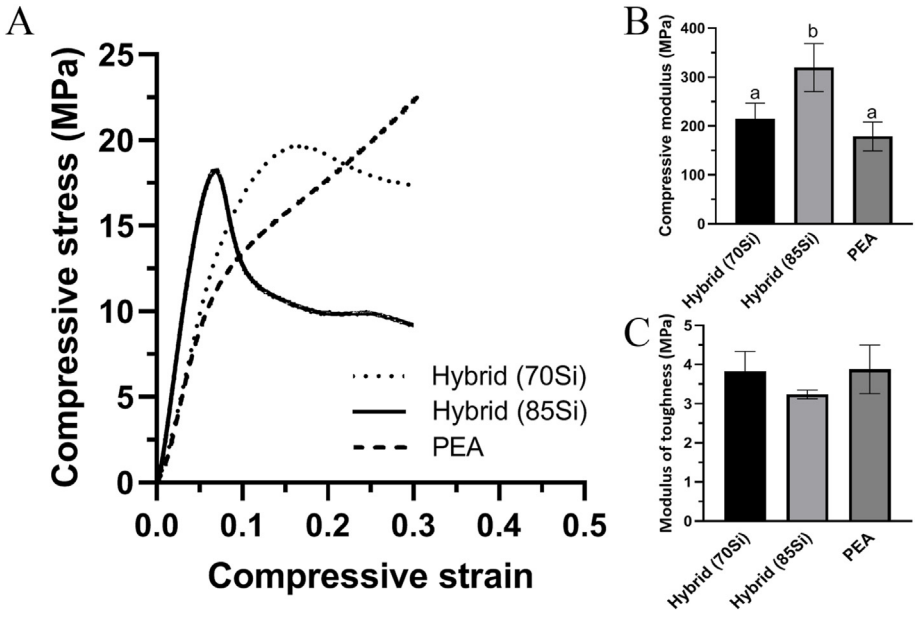

Fig. 2. Mechanical properties of PEA and hybrid materials. **(A)** Representative stress-strain curves of hybrids and PEA **(B, C)** Compressive modulus and modulus of toughness of hybrids and PEA. Modulus of toughness values were calculated by integrating stress-strain curves up to the strain of 0.3. Different letters indicate the significance at $p < 0.05$, while similar letters indicate no significance ($p > 0.05$).

anions competing for charge compensation such as boron [26], and in compositions with high P content, phosphorus appears as pyrophosphate and Si–O–P [27], and might form phosphorus-rich regions of 1.5–2 nm in size [25]. Given the fact that the network modifiers cations are consumed for charge-balancing with orthophosphate ions instead of the non-bridging oxygens, the silica network connectivity increases, and subsequently, the mechanical strength of the glass increases. Interestingly, an opposite trend was obtained in our study. It should be noted that in the cited references, the bioactive glasses underwent high-temperature thermal treatment, which is known to incorporate oxides in the glass network and increase the network connectivity. Moreover, the maximum phosphorus content in those studies was 6 mol%, while in the case of our PEA-BG (70Si), the BG contained 20% phosphorus. Since the high-temperature treatment is not feasible in the case of hybrids, we believe that the network connectivity did not change, but the higher silica content with a covalently bonded network structure comparable to the electrostatic interactions of Ca and phosphate-rich regions resulted in higher compressive modulus. The compressive modulus and modulus of toughness measured here are indicative of the effect of the presence of inorganic phase and its composition on the mechanical properties of hybrids; however, the actual mechanical properties depend on the shape of the tissue engineering construct, as well as its degradability *in vivo*. Moreover, despite the fact that here the microparticles are compressed to form cylindrical specimens, the fusion of microparticles might have not been complete in regions of specimens and this might cause more deformation under stress.

3.3. 10T1/2 cells morphology, focal adhesion formation, viability, and proliferation in culture with hybrid microparticles

The hybrid microparticles are intrinsically fluorescent due to having PEA as their organic phase [13]. This intrinsic fluorescence is used to visualize microparticles and cells around them after 4 and 7 days in culture (Fig. 3A). Cells had an intact cytoskeleton and spread on the glass slide and around the microparticles. Cell adhesion, cell shape and spreading, can regulate the differentiation lineage commitment. It has been shown that spread hMSCs committed to osteogenesis while non-spread and round cells underwent adipogenesis [28]. Interestingly,

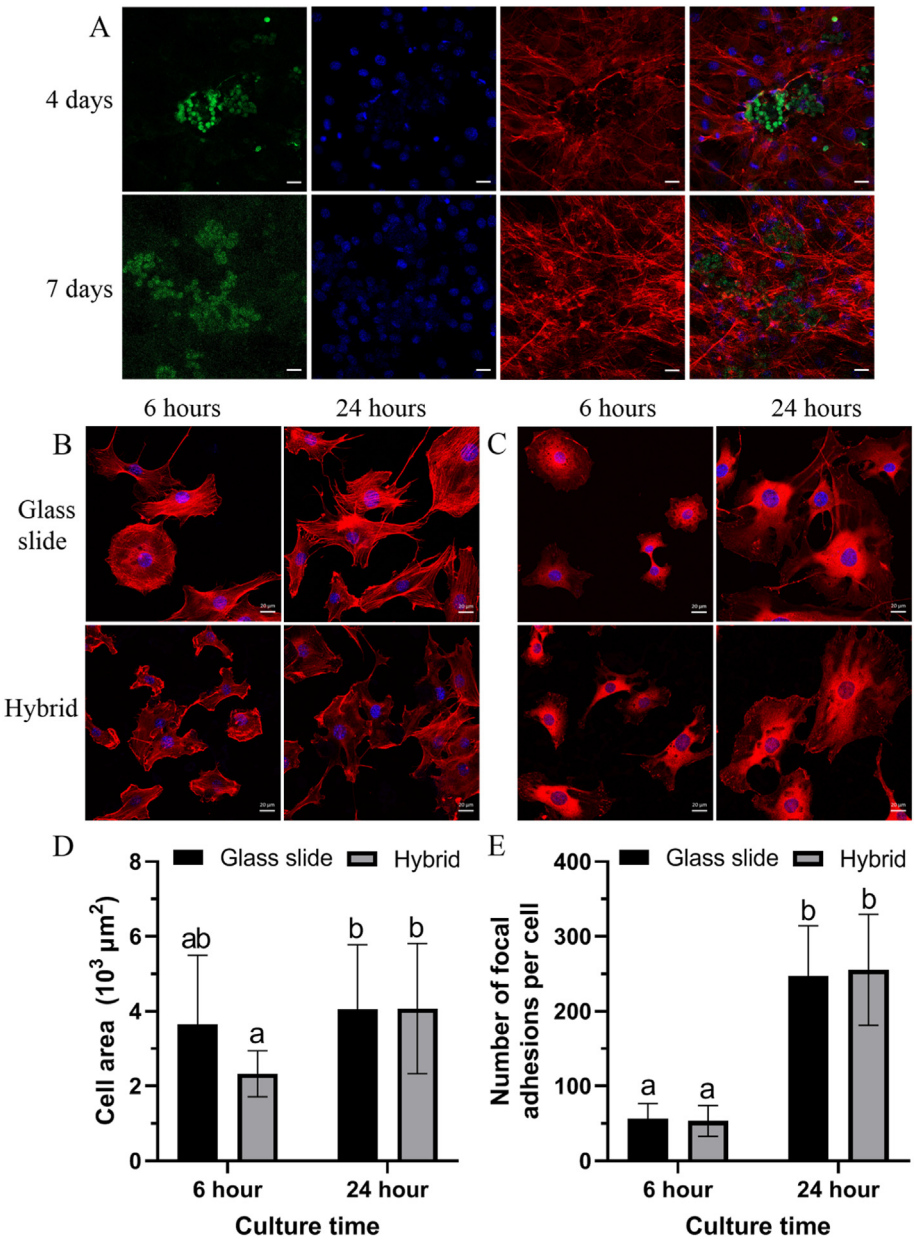

Fig. 3. 10T1/2 cells morphology and attachment. Confocal fluorescent images of **(A)** Cells cultured with hybrid microparticles for 4 and 7 days (green = intrinsic fluorescence of microparticles, blue = nuclei, red = F-actin) **(B)** Spreading of cells cultured on a glass slide and hybrid (blue = nuclei, red = F-actin) **(C)** Focal adhesions of cells cultured on a glass slide and hybrid (blue = nuclei, red = vinculin) **(D)** Measured cell area and **(E)** Number of focal adhesions per cell for cultures on glass slide and hybrid. Different letters indicate the significance at $p < 0.05$, while similar letters indicate no significance ($p > 0.05$). Scale bar = 20 μm.

direct manipulation of RhoA signaling controlled the differentiation fate of MSCs, irrespective of the differentiation media [28]. Therefore, evaluating the cell morphology in contact with biomaterials is essential in differentiation studies. In order to better visualize the adhesion of cells to the hybrid solely, cells were cultured on a film of hybrid material. Fig. 3B–E shows the spreading and adhesion of 10T1/2 cells on the hybrid material compared to the glass slide. After 6 h, cells have completely spread on glass slides with an organized cytoskeleton. After 24 h, the cell area on glass slides increased slightly. In comparison, cells on the hybrid were more rounded after 6 h. However, after 24 h, cells are well-spread with an organized cytoskeleton and a cell area comparable to the glass slide (Fig. 3B, D). Vinculin is one of the key proteins regulating focal adhesion formation and cell adhesion. In the inactive state, vinculin is located in the cytoplasm; upon recruitment for focal adhesion formation, its conformation changes, facilitating interaction with several proteins, including actin cytoskeleton [29]. The hybrid material supported the attachment of cells and formation of distinct focal adhesions at the periphery of the cells. There was no significant difference between the number of focal adhesions per cell at each time point between the glass slide and the hybrid. The number of focal adhesions increased for both substrates between 6 and 24 h (Fig. 3C, E).

The effect of hybrid microparticles on the metabolic activity of the cells was determined by the MTT assay. The metabolic activities of cultures after 1 day were normalized to tissue culture plate (TCP) as a control to determine the dose response. While the presence of microparticles caused a significant decrease in metabolic activity of cells compared to TCP after 1 day, the metabolic activity of cells was not changed significantly between concentrations of 2, 5, and 10 mg/mL (Fig. 4A). For cultures containing 20 mg/mL hybrid microparticles, the normalized metabolic activity was 71.7%. This shows that the half-maximal inhibitory concentration (IC_{50}) of hybrid microparticles is above 20 mg/mL, which is considerably higher than similar bioactive submicron particles such as silica particles (particle size = 365.1 ± 79.5 nm, IC_{50} = 34.8 μg/mL) [30], and (particle size = 760 nm, IC_{50} > 2 mg/mL) [31], and similar bioactive nanoparticles such as silica nanoparticles (particle size = 100 nm, IC_{50} = 35.9 μg/mL) [32], magnetic mesoporous silica nanoparticles (particle size = 60–80 nm, IC_{50} = 121.98 μg/mL) [33], and synthetic silicate nanoplatelets (particle size = 25–30 nm, IC_{50} = 4 mg/mL) [12]. Despite the fact that the cell type is an important factor in assessing cytotoxicity, several studies have shown that nano and submicron silica particles induce higher cytotoxicity comparable to microparticles [34–36]. Fig. 4B shows the absorbance at 570 nm after 4 and 7 days, normalized to the corresponding culture at day 1. The normalized absorbances after 4 and 7 days compared to day 1 for all the experimental groups were significantly higher. The data trend was also similar after 7 days culture compared to day 4 for TCP, 2, 5, and 10 mg/mL MP groups. These findings showed the increased metabolic activity, indicating an increased number of cells. Using resazurin assay, we also previously showed that the viability of cells embedded in 3D constructs of microparticles and fibrin gels were stable after 4- and 7-days culture for two concentrations of 20 and 80 mg/mL microparticles [13].

MTT assay measures the mitochondrial activity of the cells as a measure of cell viability. In order to directly measure cell proliferation, CyQuant Cell Proliferation Kit was used to quantify the DNA content of cultures. All cultured cells with different concentrations of microparticles showed a statistically significant increase in DNA content after 7 days, compared to day 1 of the corresponding cultures (Fig. 4C; $p < 0.05$), while there were no significant difference between the DNA content of different groups after 7 days of culture, indicating that the hybrid microparticles support the proliferation of cells. It has been reported that elevated concentrations of Ca^{2+} increased the proliferation of both 10T1/2 cells and bone marrow-derived MSCs [37]. This may be the reason for the enhanced proliferation of 10T1/2 cells in the presence of hybrid microparticles. Collectively, the results shown in Fig. 4 demonstrated that hybrid microparticles are well-tolerated by 10T1/2 cells.

3.4. Osteogenic gene expression of 10T1/2 cells

In order to evaluate the potential of hybrid microparticles to induce osteogenic differentiation, 5 mg/mL PEA-BG pristine and dexamethasone-loaded microparticles were added to 10T1/2 cells in basal culture medium without any osteogenic media supplements. Fig. 5 shows the expression of six osteogenic genes in response to pristine and dexamethasone-loaded microparticles. Runx2, also known as cbfa1 (core binding factor alpha 1), is the earliest osteogenic differentiation marker known [38]. Runx2 is also one of the upstream transcription factors of non-collagenous proteins of osteoblasts such as osteopontin (OPN), osteocalcin (OCN), and bone sialoprotein [39]. Runx2 deficient mutant mice showed a complete lack of bone formation, showing its essential role in osteogenesis [40]. Fig. 5A shows that runx2 expression is upregulated significantly after 8 h in the cultures with microparticles, while it was not upregulated in cells cultured with osteogenic media and soluble dexamethasone. It has been shown that runx2 is upregulated only after 24 h in the cultures of 10T1/2 cells under the synergistic effect of BMP2 and dexamethasone [41]. Therefore, the presence of hybrid microparticles not only led to significant upregulation of runx2 but also led to a peak at an earlier time point.

Expression of alkaline phosphatase (Alpl) is one of the known predictors of osteogenic differentiation. The elevated expression of Alpl in hard tissue formation appeared to serve two purposes: (i) decreasing the concentration of inorganic pyrophosphate, an inhibitor of mineralization, and (ii) increasing the concentration of inorganic phosphate, a promoter of mineralization [42]. After 7 days of culture, Alpl expression was upregulated significantly in culture with microparticles. Pristine microparticles resulted in 7.2-fold upregulation of Alpl, higher than the 5.4-fold observed in cultures with osteogenic media. Dexamethasone-loaded microparticles resulted in 14.6-fold Alpl upregulation, which is significantly higher than both cultures with osteogenic

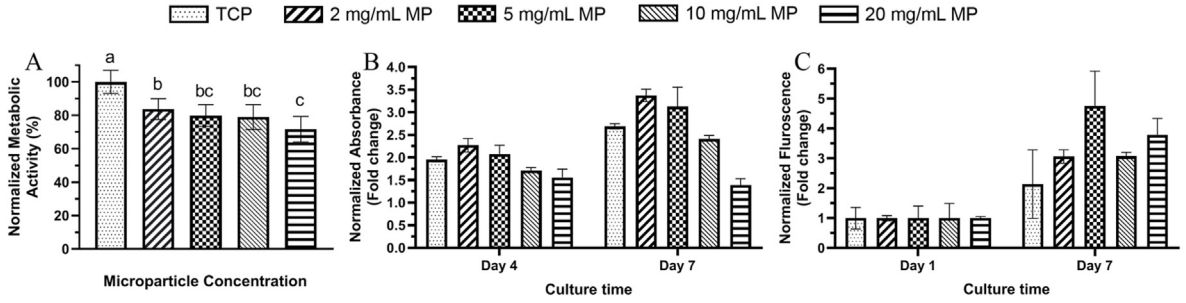

Fig. 4. Metabolic activity and proliferation of 10T1/2 cells as determined by MTT and CyQuant cell proliferation kit (n = 3). **(A)** Metabolic activity of cells cultured with different concentrations of hybrid microparticles for 1 day, normalized to tissue culture plate **(B)** Absorbance (at 570 nm) and **(C)** Cell proliferation in the presence of different concentrations of microparticles, normalized to corresponding day 1 culture. Different letters indicate the significance at $p < 0.05$, while similar letters indicate no significance ($p > 0.05$).

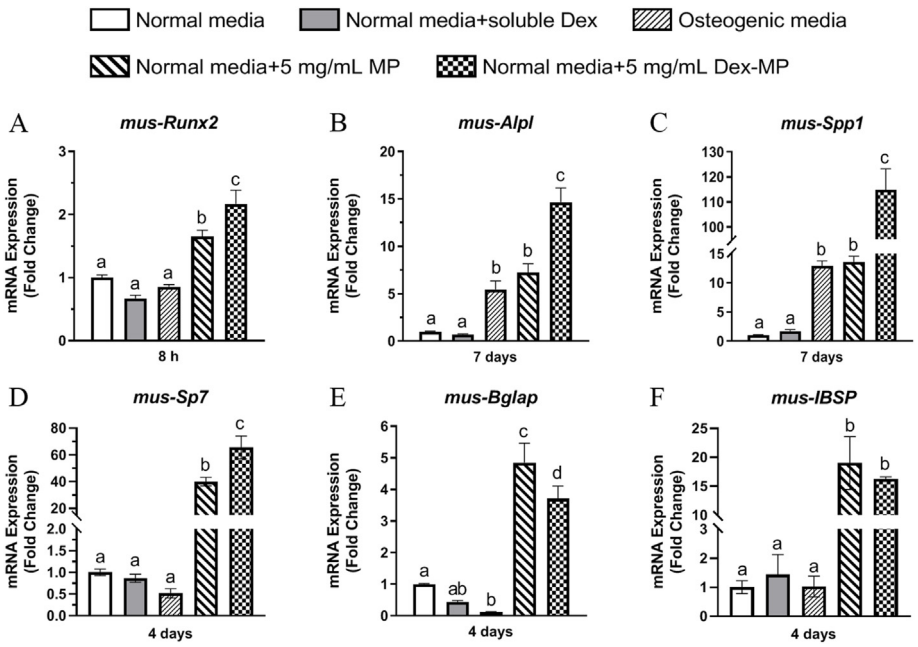

Fig. 5. 10T1/2 cells osteogenic gene expression. **(A)** Runx2 **(B)** Alpl **(C)** Spp1 **(D)** Sp7 **(E)** Bglap and **(F)** IBSP mRNA expression of 10T1/2 cells cultured with osteogenic media, normal media containing soluble dexamethasone, and normal media containing 5 mg/mL PEA-BG microparticles (n = 4). Results were normalized to GAPDH expression. Different letters indicate the significance at $p < 0.05$, while similar letters indicate no significance ($p > 0.05$).

media and unloaded microparticles (Fig. 5B). Cultures treated with soluble dexamethasone did not show any upregulation of Alpl expression.

Spp1 is the gene associated with osteopontin. Osteopontin is one of the non-collagenous proteins of the bone matrix, released from both osteoblast and osteoclast, which plays a key role in bone remodeling [43]. Similar to the observation made for Alpl, after 7 days of culture, pristine hybrid microparticles upregulated the expression of Spp1 to a level comparable to osteogenic media cultures and significantly higher than the normal media. Dexamethasone-loaded microparticles resulted in a much higher upregulation (114.8-fold) compared to other groups, while soluble dexamethasone did not lead to a significant Spp1 upregulation (Fig. 5C).

Osterix is another key transcription factor in the osteogenesis process, essential for the differentiation of pre-osteoblasts into mature osteoblasts. The absence of osterix expression in runx2 null mice suggested that osterix is downstream of runx2. In addition, in osterix null mice, no endochondral or intramembranous bone formation occurred [44]. After 4 days of culture, the expression of Sp7, the gene associated with osterix, was significantly upregulated in cultures with microparticles. Dexamethasone-loaded microparticles resulted in significantly higher upregulation compared to pristine microparticles, while no upregulation was observed in cultures with soluble dexamethasone (Fig. 5D).

Bglap is one of the genes which encodes osteocalcin. OCN is another non-collagenous protein in bone, and its synthesis is largely restricted to osteoblasts. OCN with three carboxylated glutamic acid residues has a binding affinity for Ca^{2+} and is essential for the alignment of apatite crystals in the mineralization process [45]. Here, OCN was upregulated significantly after 4 days in the presence of microparticles, while no upregulation was observed at the same time point with osteogenic media and soluble dexamethasone (Fig. 5E). Interestingly, pristine microparticles resulted in significantly higher upregulation compared to dexamethasone-loaded particles. OCN is considered a relatively late osteogenic marker, related to osteoblasts maturation and indicating the onset of mineralization. However, in cultures of bone marrow-derived human mesenchymal stromal cells on biomineralized collagen membranes [46], or osteoblast precursor MC3T3-E1 cells with bioactive glass conditioned media [47], OCN upregulation has been detected as early as 3 days. 10T1/2 cells treated with BMP7 have also shown the expression of OCN after 4 days [48]. The earlier expression of OCN may suggest that hybrid microparticles not only promoted cell differentiation but also caused cells to enter the maturation and mineralization stage at an earlier time point.

Bone sialoprotein (BSP), another major non-collagenous protein of bone extracellular matrix, is expressed primarily in mature osteoblasts at late stages of differentiation [49] and is considered as a potential nucleation site for hydroxyapatite [50]. After 4 days, the expression of IBSP, the gene associated with BSP, was significantly upregulated in cultures with microparticles, while at the same time point, in cultures with osteogenic media, and soluble dexamethasone, no upregulation was observed (Fig. 5F).

3.5. Western blot analysis

The expressions of two osteogenesis proteins were evaluated by western blot analysis after 7- and 14-days cultures (Fig. 6). Osteopontin was detected in all cultures, in both time points of 7 and 14 days; however, the expression appeared to be more pronounced in cultures with osteogenic media and dexamethasone-loaded MPs compared to cultures with pristine MPs. For all samples, the osteopontin expression was increased from 7 days to 14 days. In contrast, osteocalcin was only detected in cultures with microparticles (both pristine and

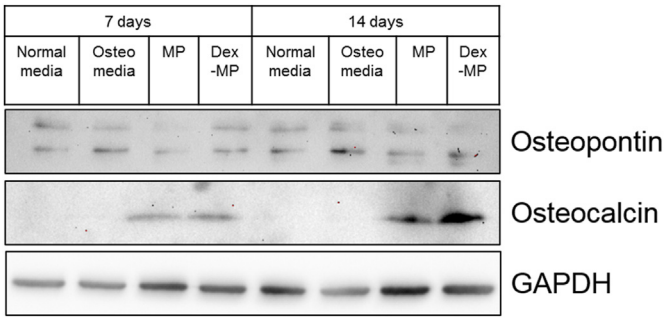

Fig. 6. Representative western blot analysis of the osteogenic proteins osteopontin and osteocalcin, following 7- and 14-days cultures.

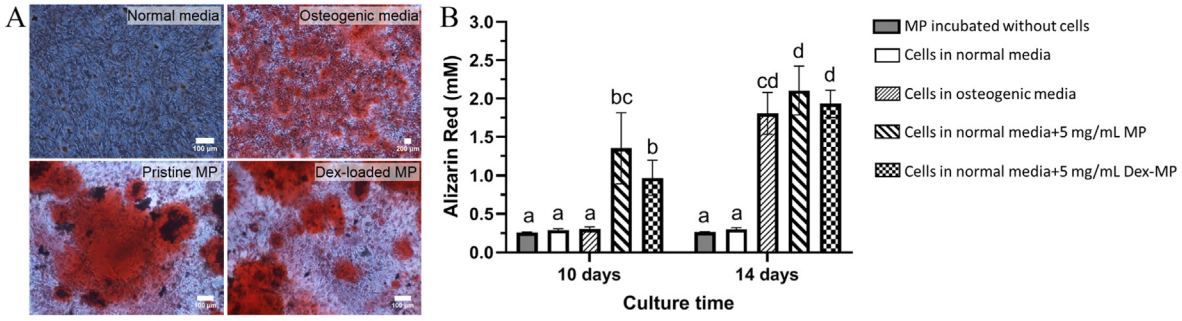

Fig. 7. Alizarin red staining of 10T1/2 cells. **(A)** Optical images showing the deposition of the mineralized matrix (stained red) on day 14 **(B)** Quantification of mineralization by extraction of alizarin red from cultures after 10- and 14-days culture (n = 6). Different letters indicate the significance at $p < 0.05$, while similar letters indicate no significance ($p > 0.05$).

dexamethasone-loaded MPs); however, the expression was robust in cultures with dexamethasone-loaded MPs. Similar to osteopontin expression, the osteocalcin protein expression was increased after 14 days compared to 7 days culture.

Osteopontin and osteocalcin are key contributors to osteogenesis and play biological and mechanical roles in bone formation. As components of the extracellular matrix, they modulate not only cell-matrix interactions but also influence matrix-mineral interaction and therefore affect bone mass, mineral size, bone structure and morphology, and presumably mechanical properties of bone [51]. In osteocalcin knockdown human mesenchymal stromal cells, mineral maturation was delayed, and the mineral to matrix ratio was significantly lower compared to the control group [52]. Mesenchymal stem cells lacking both osteocalcin and osteopontin showed reduced proliferation, reduced osteogenesis and angiogenesis potential, and delayed mineralized matrix maturation [53]. In mutant mice lacking both osteopontin and osteocalcin, significant changes in cortical area and length were observed [51]. It has been reported that exogenous supplementation of osteocalcin and osteopontin enhanced osteogenesis in both 2D and 3D culture systems as well as *in vivo* [53–55]. Therefore, the expression of osteocalcin and osteopontin is an important indicator of osteogenic differentiation of 10T1/2 cells.

3.6. Evaluation of mineralization

Mineralization of the extracellular matrix is the ultimate phenotype of osteogenic tissue. Using Alizarin red staining, the mineral formation can be detected and quantified in cultures. Osteogenic media provides an external source of phosphate (inorganic phosphate or β-glycerophosphate) to facilitate mineralization. It is believed that the dissolution of inorganic components of the hybrid microparticles provides phosphate alongside silicon and calcium ions, which potentially can substitute the external phosphate source present in the osteogenic media. Alizarin red staining of cultures after 10 days showed mineral deposition in both cases of pristine and dexamethasone-loaded microparticles, while the osteogenic media did not show any mineral deposition (Fig. 7). Alizarin red staining of microparticles incubated in PBS (in the absence of cells) for the same durations did not show any unspecific staining due to the microparticles solely. Fig. 7A shows the optical images of cultures after 14 days. After 14 days of culture, a significantly higher level of mineral deposit was observed in cultures with microparticles compared to 10 days of culture. Cultures with osteogenic media also showed mineral deposition after 14 days, to a level slightly lower than cultures with MPs (Fig. 7B). Expression of runx2 after only 8 h followed by early expression of OCN after 4 days in the case of cultures with hybrid microparticles might have resulted in early mineralization observed in cultures with microparticles after 10 days.

4. Conclusion

This study demonstrated that PEA-BG hybrid microparticles created a microenvironment that promotes osteogenic differentiation. Release of silicon, calcium, and phosphate ions from MPs, as well as loaded dexamethasone induced osteogenic differentiation in the absence of any additional factor. The hybrid microparticles also supported cell spreading and the formation of focal adhesions and cell proliferation was maintained in the presence of different concentrations of microparticles. The gene expression profile, protein expression, and mineralization studies demonstrated that a single dose of pristine or dexamethasone-loaded hybrid microparticles induced osteogenic differentiation in the absence of any media supplement. The versatility of the fluorescent microparticles may have the potential to induce not only osteogenic differentiation but also address other complications associated with bone defects such as infection through the release of suitable active agents.

Credit author statement

Neda Aslankoohi: Conceptualization, Methodology, Validation, Investigation, Formal analysis, Writing – original draft, Visualization, **Shigang Lin:** Methodology, Investigation, Validation, **Kibret Mequanint:** Conceptualization, Methodology, Writing – review & editing, Supervision, Funding acquisition.

Data availability

The raw/processed data required to reproduce these findings cannot be shared at this time due to technical or time limitations.

Declaration of competing interest

The authors declare that they have no known competing financial interests or personal relationships that could have appeared to influence the work reported in this paper.

Acknowledgment

This work was supported by the Natural Sciences and Engineering Research Council of Canada (NSERC).

References

[1] F.E. Freeman, H.Y. Stevens, P. Owens, R.E. Guldberg, L.M. McNamara, Tissue Eng. 22 (2016) 1176–1190.
[2] O. Tsigkou, J.R. Jones, J.M. Polak, M.M. Stevens, Biomaterials 30 (2009) 3542–3550.
[3] W. Li, H. Xu, X. Han, S. Sun, Q. Chai, X. Xu, Z. Man, Colloids Surf. B Biointerfaces 192 (2020) 111040.
[4] A.B. Faia-Torres, M. Charnley, T. Goren, S. Guimond-Lischer, M. Rottmar, K. Maniura-Weber, N.D. Spencer, R.L. Reis, M. Textor, N.M. Neves, Acta Biomater. 28 (2015) 64–75.

[5] M.J. Kim, B. Lee, K. Yang, J. Park, S. Jeon, S.H. Um, D.I. Kim, S.G. Im, S.-W. Cho, Biomaterials 34 (2013) 7236–7246.
[6] N. Aslankoohi, D. Mondal, A.S. Rizkalla, K. Mequanint, Polymers 11 (2019) 1437.
[7] N. Aslankoohi, K. Mequanint, ACS Appl. Bio Mat. 3 (2020) 3621–3630.
[8] M.T. Tavares, M.B. Oliveira, V.M. Gaspar, J.F. Mano, J.P.S. Farinha, C. Baleizão, Adv. Biosys. 4 (2020) 2000123.
[9] M.T. Tavares, M.B. Oliveira, J.F. Mano, J.P.S. Farinha, C. Baleizão, Mater. Sci. Eng. C 107 (2020) 110348.
[10] Á.J. Leite, A.I. Gonçalves, M.T. Rodrigues, M.E. Gomes, J.F. Mano, ACS Appl. Mater. Interfaces 10 (2018) 23311–23320.
[11] M. Ojansivu, S. Vanhatupa, L. Björkvik, H. Häkkänen, M. Kellomäki, R. Autio, J.A. Ihalainen, L. Hupa, S. Miettinen, Acta Biomater. 21 (2015) 190–203.
[12] A.K. Gaharwar, S.M. Mihaila, A. Swami, A. Patel, S. Sant, R.L. Reis, A.P. Marques, M.E. Gomes, A. Khademhosseini, Adv. Mater. 25 (2013) 3329–3336.
[13] N. Aslankoohi, K. Mequanint, Mater. Sci. Eng. C 128 (2021) 112288.
[14] D.K. Knight, E.R. Gillies, K. Mequanint, Biomacromolecules 12 (2011) 2475–2487.
[15] V.C. Talayero, M. Vicente-Manzanares, Multiparametric analysis of focal adhesions in bidimensional substrates, in: M. Vicente-Manzanares (Ed.), The Integrin Interactome: Methods and Protocols, Springer US, New York, NY, 2021, pp. 27–37.
[16] C.A. Gregory, W.G. Gunn, A. Peister, D.J. Prockop, Anal. Biochem. 329 (2004) 77–84.
[17] K. Qiu, B. Chen, W. Nie, X. Zhou, W. Feng, W. Wang, L. Chen, X. Mo, Y. Wei, C. He, ACS Appl. Mater. Interfaces 8 (2016) 4137–4148.
[18] S. Yang, M. Wang, H. Zhang, K.-y. Cai, X.-k. Shen, F. Deng, Y. Zhang, L. Wang, RSC Adv. 4 (2014) 65163–65172.
[19] D.K. Knight, E.R. Gillies, K. Mequanint, Acta Biomater. 10 (2014) 3484–3496.
[20] J.J. Chung, S. Li, M.M. Stevens, T.K. Georgiou, J.R. Jones, Chem. Mater. 28 (2016) 6127–6135.
[21] D. Mondal, S.J. Dixon, K. Mequanint, A.S. Rizkalla, J. Mech. Behavior Biomed. Mat. 75 (2017) 180–189.
[22] B.A. Allo, A.S. Rizkalla, K. Mequanint, ACS Appl. Mater. Interfaces 4 (2012) 3148–3156.
[23] T. Sang, S. Li, H.-K. Ting, M.M. Stevens, C.R. Becer, J.R. Jones, Chem. Mater. 30 (2018) 3743–3751.
[24] M. Dziadek, B. Zagrajczuk, P. Jelen, Z. Olejniczak, K. Cholewa-Kowalska, Ceram. Int. 42 (2016) 14700–14709.
[25] R. Mathew, C. Turdean-Ionescu, B. Stevensson, I. Izquierdo-Barba, A. García, D. Arcos, M. Vallet-Regí, M. Edén, Chem. Mater. 25 (2013) 1877–1885.
[26] L. Deilmann, O. Winter, B. Cerrutti, H. Bradtmüller, C. Herzig, A. Limbeck, O. Lahayne, C. Hellmich, H. Eckert, D. Eder, J. Mater. Chem. B 8 (2020) 1456–1465.
[27] A. Tilocca, A.N. Cormack, J. Phys. Chem. B 111 (2007) 14256–14264.
[28] R. McBeath, D.M. Pirone, C.M. Nelson, K. Bhadriraju, C.S. Chen, Dev. Cell 6 (2004) 483–495.
[29] J.D. Humphries, P. Wang, C. Streuli, B. Geiger, M.J. Humphries, C. Ballestrem, J. Cell Biol. 179 (2007) 1043–1057.
[30] X. Yang, J. Liu, H. He, L. Zhou, C. Gong, X. Wang, L. Yang, J. Yuan, H. Huang, L. He, B. Zhang, Z. Zhuang, Part. Fibre Toxicol. 7 (2010) 1. https://particleandfibretoxicology.biomedcentral.com/articles/10.1186/1743-8977-7-1.
[31] H. Yuan, F. Gao, Z. Zhang, L. Miao, R. Yu, H. Zhao, M. Lan, J. Health Sci. 56 (2010) 632–640.
[32] C. Gong, G. Tao, L. Yang, J. Liu, H. He, Z. Zhuang, Mol. Biol. Rep. 39 (2012) 4915–4925.
[33] G.B. Heggannavar, C.G. Hiremath, D.D. Achari, V.G. Pangarkar, M.Y. Karidurаganavar, ACS Omega 3 (2018) 8017–8026.
[34] T. Kusaka, M. Nakayama, K. Nakamura, M. Ishimiya, E. Furusawa, K. Ogasawara, PLoS One 9 (2014), e92634.
[35] Y. Xue, Q. Chen, T. Ding, J. Sun, Int. J. Nanomed. 9 (2014) 2891–2903.
[36] Y. Kamikubo, T. Yamana, Y. Hashimoto, T. Sakurai, ACS Chem. Neurosci. 10 (2019) 304–312.
[37] M.N. Lee, H.-S. Hwang, S.-H. Oh, A. Roshanzadeh, J.-W. Kim, J.H. Song, E.-S. Kim, J.-T. Koh, Exp. Mol. Med. 50 (2018). https://www.nature.com/articles/s12276-018-0170-6.
[38] J.E. Aubin, J.T. Triffitt, Chapter 4 - mesenchymal stem cells and osteoblast differentiation, in: J.P. Bilezikian, L.G. Raisz, G.A. Rodan (Eds.), Principles of Bone Biology, second ed., Academic Press, San Diego, 2002, pp. 59–81.
[39] P. Ducy, Dev. Dynam. 219 (2000) 461–471.
[40] T. Komori, H. Yagi, S. Nomura, A. Yamaguchi, K. Sasaki, K. Deguchi, Y. Shimizu, R.T. Bronson, Y.H. Gao, M. Inada, M. Sato, R. Okamoto, Y. Kitamura, S. Yoshiki, T. Kishimoto, Cell 89 (1997) 755–764.
[41] Y. Mikami, M. Asano, M.J. Honda, M. Takagi, J. Cell. Physiol. 223 (2010) 123–133.
[42] E.E. Golub, K. Boesze-Battaglia, Curr. Opin. Orthop. 18 (2007). https://journals.lww.com/co-ortho/fulltext/2007/09000/the_role_of_alkaline_phosphatase_in_mineralization.5.aspx.
[43] M.A. Icer, M. Gezmen-Karadag, Clin. Biochem. 59 (2018) 17–24.
[44] K. Nakashima, X. Zhou, G. Kunkel, Z. Zhang, J.M. Deng, R.R. Behringer, B. de Crombrugghe, Cell 108 (2002) 17–29.
[45] T. Moriishi, R. Ozasa, T. Ishimoto, T. Nakano, T. Hasegawa, T. Miyazaki, W. Liu, R. Fukuyama, Y. Wang, H. Komori, X. Qin, N. Amizuka, T. Komori, PLoS Genet. 16 (2020), e1008586.
[46] D. de Melo Pereira, M. Eischen-Loges, Z.T. Birgani, P. Habibovic, Front Bioeng Biotechnol 8 (2020) 554565.
[47] V.G. Varanasi, E. Saiz, P.M. Loomer, B. Ancheta, N. Uritani, S.P. Ho, A.P. Tomsia, S.J. Marshall, G.W. Marshall, Acta Biomater. 5 (2009) 3536–3547.
[48] P. Ducy, R. Zhang, V. Geoffroy, A.L. Ridall, G. Karsenty, Cell 89 (1997) 747–754.
[49] P. Bianco, L.W. Fisher, M.F. Young, J.D. Termine, P.G. Robey, Calcif. Tissue Int. 49 (1991) 421–426.
[50] B. Ganss, R.H. Kim, J. Sodek, Crit. Rev. Oral Biol. Med. 10 (1999) 79–98.
[51] S. Bailey, G. Karsenty, C. Gundberg, D. Vashishth, Ann. N. Y. Acad. Sci. 1409 (2017) 79–84.
[52] Y.T. Tsao, Y.J. Huang, H.H. Wu, Y.A. Liu, Y.S. Liu, O.K. Lee, Int. J. Mol. Sci. 18 (2017). https://www.mdpi.com/1422-0067/18/1/159.
[53] M.S. Carvalho, J.C. Silva, C.M. Hoff, J.M.S. Cabral, R.J. Linhardt, C.L. da Silva, D. Vashishth, J. Cell. Physiol. 235 (2020) 7496–7515.
[54] M.S. Carvalho, A.A. Poundarik, J.M.S. Cabral, C.L. da Silva, D. Vashishth, Sci. Rep. 8 (2018) 14388.
[55] M.S. Carvalho, J.M.S. Cabral, C.L. da Silva, D. Vashishth, J. Cell. Biochem. 120 (2019) 6555–6569.